Angewandte Zuschriften

Chemical Imaging of Materials

DOI: 10.1002/ange.201309295

Assessing Chemical Heterogeneity at the Nanoscale in Mixed-Ligand Metal–Organic Frameworks with the PTIR Technique**

*Aaron M. Katzenmeyer, Jerome Canivet, Glenn Holland, David Farrusseng, and Andrea Centrone**

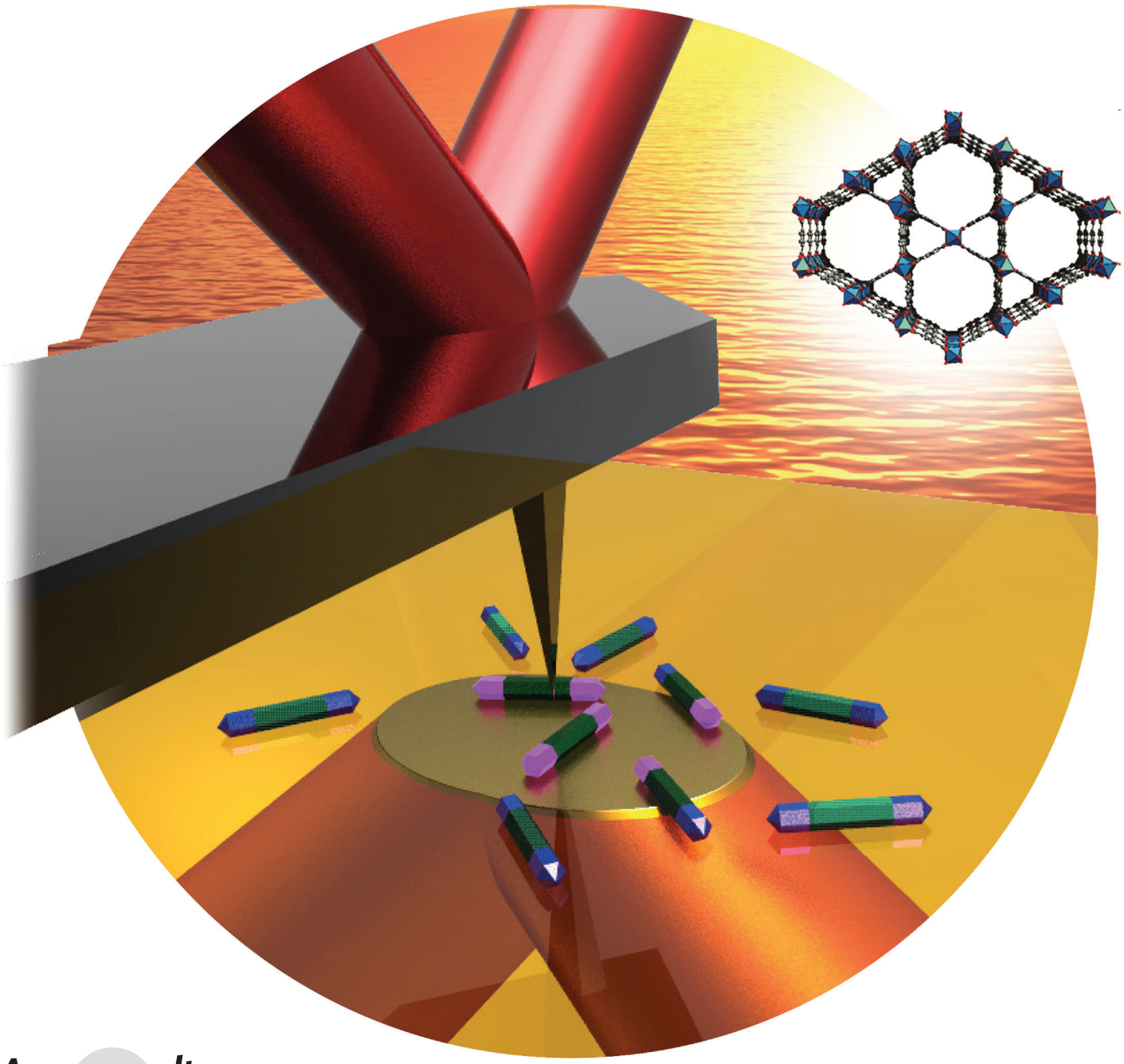

Angewandte Chemie

Abstract: *Recently, the use of mixtures of organic-building-block linkers has given chemists an additional degree of freedom for engineering metal–organic frameworks (MOFs) with specific properties; however, the poor characterization of the chemical complexity of such MixMOF structures by conventional techniques hinders the verification of rational design. Herein, we describe the application of a technique known as photothermal induced resonance to individual MixMOF microcrystals to elucidate their chemical composition with nanoscale resolution. Results show that MixMOFs isoreticular to In-MIL-68, obtained either directly from solution or by postsynthetic linker exchange, are homogeneous down to approximately 100 nm. Additionally, we report a novel in situ process that enables the engineering of anisotropic domains in MOF crystals with submicron linker-concentration gradients.*

Metal–organic frameworks (MOFs), also known as porous coordination polymers, are crystalline, micro- to mesoporous functional materials consisting of inorganic clusters interconnected by organic linkers. The possibility of tailoring the chemical functionality and pore size while maintaining the framework structure, a concept termed isoreticularity,[1] makes these materials promising for adsorption-based processes,[2] heat pumps,[3] catalysis,[4] and particularly photocatalysis,[5] gas storage,[6] drug delivery,[7] sensing,[8] and imaging.[9] To target those applications, isoreticular MOFs composed of mixtures of linkers (referred to as multivariate MOFs or MixMOFs), including core–shell structures,[10] are one of the latest achievements in the field.[4a,6,11] However, along with the benefits of multivariate-MOF complexity comes the challenge of spatially resolving the distribution of the constituent building blocks within MOF crystallites. For example, homogeneity in the distribution of active or adsorption sites within a crystal is a prerequisite for the design of advanced catalytic materials[12] or sensing. However, the determination of the chemical composition at the nanoscale in such materials remains elusive owing to the limited spatial resolution of conventional techniques. This lack of spatially resolved information hinders fundamental understanding of these materials and consequently the ability to engineer them for greatest efficacy. In this study, the local chemical composition of individual MixMOF microcrystals was determined for the first time with nanoscale resolution by using the photothermal induced resonance (PTIR) technique,[13] a novel method that combines the lateral resolution of atomic force microscopy (AFM) with the chemical specificity of infrared (IR) spectroscopy (Figure 1). PTIR experiments show that MixMOFs isoreticular to In-MIL-68,[14] made either directly from solution or by postsynthetic linker exchange, are homogeneous down to a length scale of approximately 100 nm. Additionally, an in situ process for engineering anisotropic domains in MOF crystals is reported leading to a linker-concentration gradient occurring within approximately 600 nm.

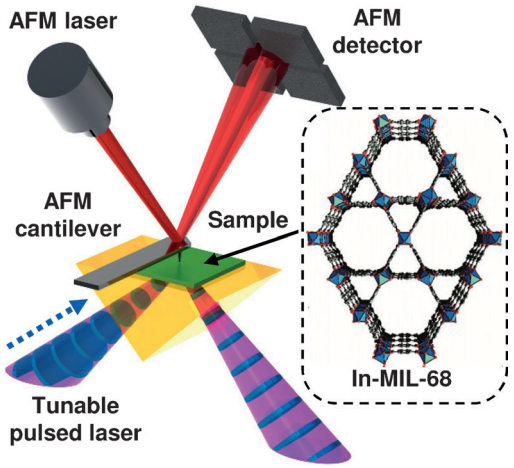

Figure 1. Schematic illustration of the PTIR technique: The IR laser beam (envelope in pink) illuminates the sample through total internal reflection. Absorption in the sample results in thermal expansion and deflection of the AFM cantilever. The inset depicts the crystal structure of In-MIL-68.

MixMOF characterization has been attempted with a variety of techniques. High-resolution XRD was used to demonstrate the homogeneity of "mixed" Al-MIL-53[11a] and MOF-5[4a] crystals in which the terephthalate (bdc) linker is partially substituted by 2-aminoterephthalate (abdc). However, powder XRD cannot assess linker gradients within a crystal or distinguish a physical mixture of crystals from chemically distinct domains within a crystal. Visible images and IR microspectroscopy were used to prove the formation of a MOF (crystals $>200\,\mu m$) in which two linkers form phase-separated domains.[15] However, the resolution of these techniques is insufficient for many technologically relevant MOFs, which grow preferentially as nano- or microcrystals, or in applications for which large crystals may be undesirable. Energy-dispersive X-ray spectroscopy was used to assess the elemental composition of MOFs with submicron resolution,[16] but this technique cannot identify functional groups nor confirm the incorporation of the linker(s) in the MOF structure. Furthermore, electron beams are known to damage MOFs.[17] Very recently, solid-state NMR spectroscopy and molecular simulations were used to distinguish (on average) between alternating, random, and cluster ligand distribution in MixMOFs isoreticular to MOF-5.[18] This indirect approach is certainly a step forward in the characterization of MixMOFs but does not provide spatial information on the ligand distribution within a crystal. The PTIR technique was applied in this work to overcome these limitations and determine the

[*] Dr. A. M. Katzenmeyer, G. Holland, Dr. A. Centrone
Center for Nanoscale Science and Technology
National Institute of Standards and Technology
100 Bureau Drive, Gaithersburg, MD 20899 (USA)
E-mail: andrea.centrone@nist.gov
Dr. J. Canivet, Dr. D. Farrusseng
Institut de Recherches sur la Catalyse et l'Environnement de Lyon (IRCELYON), Université Lyon 1, CNRS
2, Avenue Albert Einstein, 69626 Villeurbanne (France)

[**] PTIR = photothermal induced resonance.

Supporting information for this article is available on the WWW under http://dx.doi.org/10.1002/anie.201309295.

nanoscale linker heterogeneity in amino-containing bifunctional MOF crystals.

In the PTIR technique, also known as AFM–IR, the sample is placed on an optical prism and illuminated by total internal reflection with a pulsed tunable IR laser, while a contact AFM tip extracts the local chemical composition (Figure 1). Our PTIR setup uses two pulsed laser sources tunable between 1.55 (6650 cm^{-1}) and 16.00 μm (625 cm^{-1}). The absorption of a laser pulse in the sample results in local heating, sample expansion, and excitation of the AFM cantilever motion, which is monitored by a four-quadrant photodetector. The local IR spectrum is obtained by plotting the maximum amplitude of the cantilever deflection as a function of the wavelength. PTIR chemical maps are obtained by illuminating the sample at a fixed wavelength while the AFM tip scans the sample. The typical laser spot size is approximately 30 μm, but the AFM tip acts as a "spatial filter" allowing the extraction of spectroscopic information with nanoscale resolution,[13b] several times smaller than the diffraction limit of IR light. Since the PTIR signal is proportional to the absorbed energy,[13b] PTIR spectra can be used for material identification by comparison with IR-spectral libraries.[19] For thin samples (< 1 μm), the PTIR signal increases linearly with sample thickness,[13b] while the sensing mechanism (probe actuation) makes samples with large linear-expansion coefficients (α), such as polymers[13b,20] or biological samples,[13a,21] easier to characterize. This study demonstrates that MOFs, which typically have relatively small and negative α,[22] are also amenable to PTIR characterization.

MIL-68 exhibits a rod-shaped structure formed by indium octahedra and terephthalates as bridging linkers[14] and contains hexahedral and triangular 1D channels with apertures of 1.6 and 0.6 nm, respectively (Figure 1, inset). The samples contain pure bdc or abdc linker or a mixture of two and are obtained either solvothermally from a solution or by postsynthetic ligand exchange.[23] Depending on the synthetic conditions, homogeneous or gradient compositions can be obtained (see below). Homolinker samples of In-MIL-68 (sample **I**, bdc linker) and In-MIL-68-NH_2 (sample **II**, abdc linker) were synthesized according to previously reported procedures and used as references.[14,24] Three mixed-linker In-MIL-68 samples made from bdc and abdc were synthesized by different methods (Table 1). Crystallization from a solution containing an equal concentration of bdc and abdc linkers yielded rod-shaped crystals tens of microns in length of corresponding composition (sample **III**). Similarly to previously reported methods of postsynthetic ligand exchange,[23c] placing In-MIL-68 seed rods in a solution containing abdc at 100 °C for 48 h yielded a material with an average bdc/abdc linker composition of 2:1 for **IV**.

To achieve ligand anisotropy within the In-MIL-68 isoreticular structure, a spatially confined, in situ sequential synthesis was devised and carried out under conditions similar to those reported previously.[24a] The confinement allows monitoring the growth in situ with an optical microscope and suppresses the seeded vertical growth of the crystals, which could complicate PTIR characterization. In-MIL-68 seed crystals were grown directly on the ZnSe prism under 2D physical confinement. Two solutions of indium and the desired linker were sequentially added and heated; the initial In-MIL-68 crystals acted as a seed for the secondary growth of In-MIL-68-NH_2 (**V**). All samples (**I**–**V**) were characterized by PTIR to determine the distribution of organic linkers in the MOF framework. In a typical experiment (for **I**–**IV**), a dilute methanolic suspension prepared from activated MOF powder was cast on a ZnSe prism and allowed to dry before the PTIR measurement. After recording the AFM height image, the AFM tip was moved to various locations on the crystal, and PTIR spectra were collected at each location.

Representative PTIR spectra of monoligand MOF samples **I** and **II** show common and distinctive absorption peaks (Figure 2). The C–H out-of-plane bending frequencies (around 700 cm^{-1}) are widely used in IR spectroscopy to identify the position and number of chemical substitutions in aromatic rings.[25] Not surprisingly, the two MOFs show distinct peaks in this region, at 742 cm^{-1} for **I** and at 762 cm^{-1} for **II**. A peak at 1260 cm^{-1}, characteristic of the

Table 1: Preparation of MIL-68 samples.[a]

Synthetic method	Sample	Linker composition[b]
crystallization from solution	**I**	bdc
crystallization from solution	**II**	abdc
crystallization from solution	**III**	bdc/abdc (1:1)
Post-synthetic ligand exchange	**IV**	bdc/abdc (2:1)
sequential growth	**V**	not determined

[a] Synthesis details are reported in the Supporting Information. [b] The linker composition was determined by liquid-state ^{1}H NMR spectroscopy of a dissolved MOF sample.

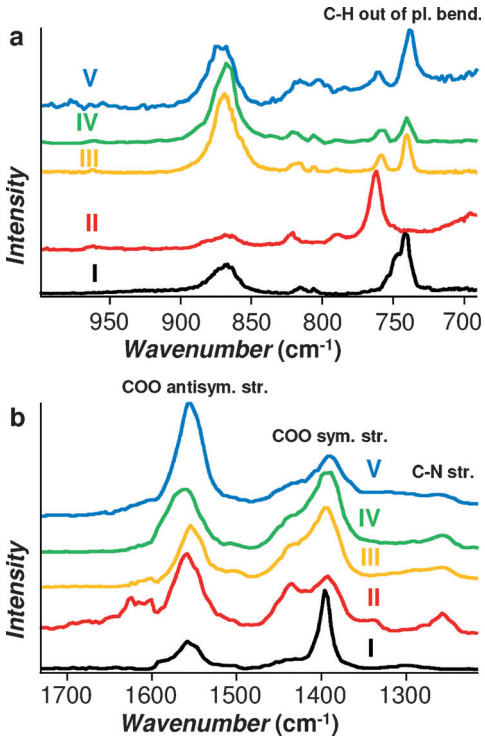

Figure 2. a,b) Representative PTIR spectra for MIL-68 samples **I**–**V**. The spectra are displayed with an offset for clarity.

C–N stretching, is observed in the spectrum of **II** and it is of course absent in the spectrum of **I**. The peaks at 1390 and 1556 cm^{-1}, assigned to the symmetric and antisymmetric carboxylate stretching,[24a] prove that the ligands are part of the framework and are not just adsorbates. This conclusion is supported by the absence of a peak around 1672 cm^{-1}, characteristic of uncoordinated carboxylic groups in these ligands (Figure 2; see also Figures S4 and S5 in the Supporting Information).

The spectra of sample **III** resemble a combination of the spectra for the two homoligand MOFs (Figure 2). PTIR spectra collected near the center, near the tip, and on the tip of a crystal of **III** are essentially identical, indicating ligand homogeneity (Figure 3).

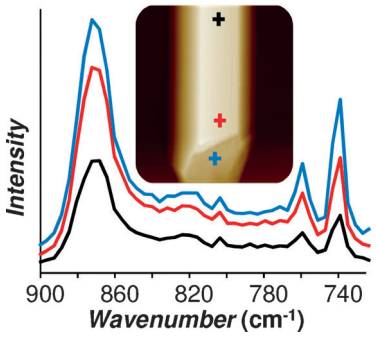

Figure 3. PTIR spectra of **III** taken at the color-coded locations denoted in the AFM height image (inset). The spectra are displayed with an offset for clarity.

The PTIR spectra of the ligand-exchanged sample **IV** resemble the spectra of **III** (Figure 2). Chemical maps (see Figure S6) of crystals of **IV** also show homogeneity of linker distribution. We believe that the ligand homogeneity in these samples results from the ease of ligand exchange in MOFs isoreticular to In-MIL-68.[23b] Our data suggest that ligand exchange occurs homogeneously throughout the crystals under the synthetic conditions used here. PTIR spectra from all samples compare favorably with those recorded at the macroscale with a FTIR spectrometer (see Figure S4).

The growth of **V** was monitored in situ with an optical microscope (see Figure S7). During secondary growth, the crystals grew several microns in the direction of the long, *c* axis and minimally in width. The same crystals were readily located by using an optical microscope integrated with the PTIR setup. PTIR spectra (Figure 2) reveal that both ligands are present throughout these crystals, suggesting that some ligand exchange takes place in the seed crystal (see Figure S8). However, chemical maps of **V** reveal a lengthwise heterogeneous distribution of ligands (Figure 4).

Two crystals of **V** (identified by arrows in Figure S7 of the Supporting Information) were imaged: one in its entirety at moderate spatial resolution (Figure 4a–c) and one near the tip at high resolution (Figure 4d–f). The insets in Figure 4 show the PTIR intensity profiles over the long axis of the MOF crystals. The maps of the abdc C–N stretch at 1260 cm^{-1} (Figure 4b,e) show stronger intensity at the crystal ends,

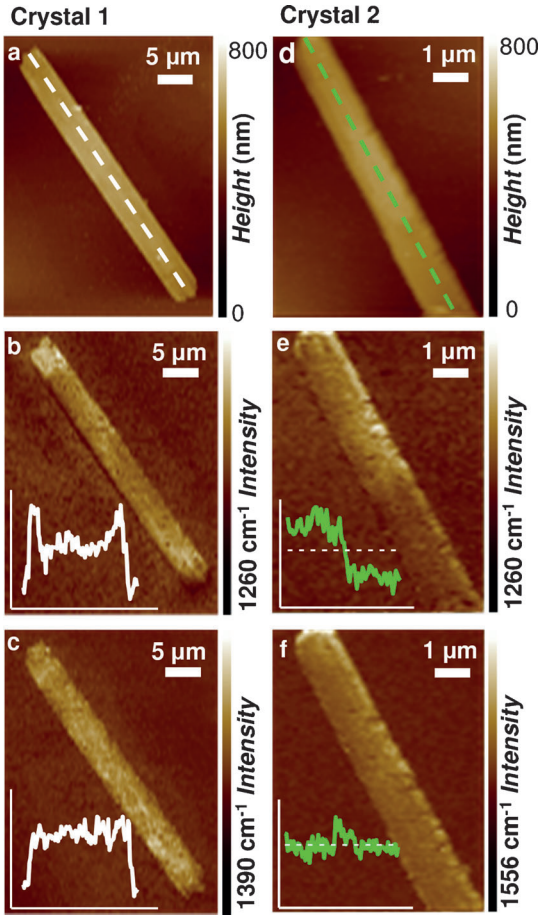

Figure 4. a) Moderate-resolution AFM height image, b) PTIR map of the C–N stretch, and c) PTIR map of the common symmetric carboxylate stretch for the crystal designated by the white arrow in Figure S7 of the Supporting Information. d) High-resolution AFM height image, e) PTIR map of the C–N stretch, and f) PTIR map of the common antisymmetric carboxylate stretch for the crystal designated by the green arrow in Figure S7. Insets are PTIR intensity profiles along the long axis of the crystal, as indicated by the dashed lines in the height images. The dashed lines in (e,f) are a guide only.

indicating that the material grown on the seed crystals is richer in the aminated ligand as compared to the seed. Chemical maps of the common carboxylate stretching frequencies (Figure 4c,f) show the expected uniformity of this moiety and confirm (along with the absence of a measureable peak at 1672 cm^{-1}) that the abdc ligand comprises the framework. The high-resolution (100 nm) map of the C–N stretch reveals a fairly abrupt concentration gradient, occurring within approximately 600 nm (Figure 4e). In contrast, the map of the common antisymmetric carboxylate stretch shows no gradient (Figure 4f).

In conclusion, we have presented a novel in situ process for engineering submicron linker anisotropy in MixMOFs. The PTIR technique enables imaging heterogeneous and homogeneous domains in MOF single crystallites with nanoscale resolution and enables determining the extent of linker gradients between MOF domains. Furthermore, the previously postulated linker homogeneity of In-MIL-68 MixMOFs obtained from direct crystallization and postsynthetic linker

exchange was proven unambiguously.[23] This finding is of particular relevance because uniform distribution of active sites is a prerequisite for the preparation of efficient catalysts and sensors. Such proof, together with the extended and ordered MOF molecular structures, reinforces the belief that MOFs may be used as model catalyst materials whose active sites can, in principle, be characterized as completely as those of molecular species. We believe that the proofs of concept presented here will foster MixMOF research, leading to better understanding of these materials and consequently help engineer them for greatest efficacy.

Received: October 24, 2013
Revised: January 23, 2014
Published online: February 24, 2014

Keywords: atomic force microscopy · IR spectroscopy · multivariate metal–organic frameworks · nanoscale chemical imaging · photothermal induced resonance

[1] a) M. Eddaoudi, J. Kim, N. Rosi, D. Vodak, J. Wachter, M. O'Keeffe, O. M. Yaghi, *Science* **2002**, *295*, 469 – 472; b) L. Ma, J. M. Falkowski, C. Abney, W. Lin, *Nat. Chem.* **2010**, *2*, 838 – 846.

[2] a) L. Alaerts, M. Maes, L. Giebeler, P. A. Jacobs, J. A. Martens, J. F. M. Denayer, C. E. A. Kirschhock, D. E. De Vos, *J. Am. Chem. Soc.* **2008**, *130*, 14170 – 14178; b) A. Centrone, E. E. Santiso, T. A. Hatton, *Small* **2011**, *7*, 2356 – 2364.

[3] S. K. Henninger, H. A. Habib, C. Janiak, *J. Am. Chem. Soc.* **2009**, *131*, 2776 – 2777.

[4] a) W. Kleist, M. Maciejewski, A. Baiker, *Thermochim. Acta* **2010**, *499*, 71 – 78; b) J. Lee, O. K. Farha, J. Roberts, K. A. Scheidt, S. T. Nguyen, J. T. Hupp, *Chem. Soc. Rev.* **2009**, *38*, 1450 – 1459.

[5] a) A. Fateeva, P. A. Chater, C. P. Ireland, A. A. Tahir, Y. Z. Khimyak, P. V. Wiper, J. R. Darwent, M. J. Rosseinsky, *Angew. Chem.* **2012**, *124*, 7558 – 7562; *Angew. Chem. Int. Ed.* **2012**, *51*, 7440 – 7444; b) Y. Fu, D. Sun, Y. Chen, R. Huang, Z. Ding, X. Fu, Z. Li, *Angew. Chem.* **2012**, *124*, 3420 – 3423; *Angew. Chem. Int. Ed.* **2012**, *51*, 3364 – 3367; c) P. Wu, C. He, J. Wang, X. Peng, X. Li, Y. An, C. Duan, *J. Am. Chem. Soc.* **2012**, *134*, 14991 – 14999; d) M. Dan-Hardi, C. Serre, T. Frot, L. Rozes, G. Maurin, C. Sanchez, G. Férey, *J. Am. Chem. Soc.* **2009**, *131*, 10857 – 10858.

[6] H. Deng, C. J. Doonan, H. Furukawa, R. B. Ferreira, J. Towne, C. B. Knobler, B. Wang, O. M. Yaghi, *Science* **2010**, *327*, 846 – 850.

[7] P. Horcajada, T. Chalati, C. Serre, B. Gillet, C. Sebrie, T. Baati, J. F. Eubank, D. Heurtaux, P. Clayette, C. Kreuz, J.-S. Chang, Y. K. Hwang, V. Marsaud, P.-N. Bories, L. Cynober, S. Gil, G. Férey, P. Couvreur, R. Gref, *Nat. Mater.* **2010**, *9*, 172 – 178.

[8] L. E. Kreno, K. Leong, O. K. Farha, M. Allendorf, R. P. Van Duyne, J. T. Hupp, *Chem. Rev.* **2012**, *112*, 1105 – 1125.

[9] a) W. Xuan, C. Zhu, Y. Liu, Y. Cui, *Chem. Soc. Rev.* **2012**, *41*, 1677 – 1695; b) J. Della Rocca, D. Liu, W. Lin, *Acc. Chem. Res.* **2011**, *44*, 957 – 968.

[10] a) S. Furukawa, .K. Hirai, K. Nakagawa, Y. Takashima, R. Matsuda, T. Tsuruoka, M. Kondo, R. Haruki, D. Tanaka, H. Sakamoto, S. Shimomura, O. Sakata, S. Kitagawa, *Angew. Chem.* **2009**, *121*, 1798 – 1802; *Angew. Chem. Int. Ed.* **2009**, *48*, 1766 – 1770; b) X. Song, T. K. Kim, H. Kim, D. Kim, S. Jeong, H. R. Moon, M. S. Lah, *Chem. Mater.* **2012**, *24*, 3065 – 3073; c) K. Koh, A. G. Wong-Foy, A. J. Matzger, *Chem. Commun.* **2009**, 6162 – 6164.

[11] a) S. Marx, W. Kleist, J. Huang, M. Maciejewski, A. Baiker, *Dalton Trans.* **2010**, *39*, 3795 – 3798; b) A. A. Talin, A. Centrone, A. C. Ford, M. E. Foster, V. Stavila, P. Haney, R. A. Kinney, V. Szalai, F. El Gabaly, H. P. Yoon, F. Léonard, M. D. Allendorf, *Science* **2014**, *343*, 66 – 69.

[12] U. Díaz, M. Boronat, A. Corma, *Proc. R. Soc. London Ser. A* **2012**, *468*, 1927 – 1954.

[13] a) A. Dazzi, R. Prazeres, F. Glotin, J. M. Ortega, M. Al-Sawaftah, M. de Frutos, *Ultramicroscopy* **2008**, *108*, 635 – 641; b) B. Lahiri, G. Holland, A. Centrone, *Small* **2013**, *9*, 439 – 445; c) B. Lahiri, G. Holland, V. Aksyuk, A. Centrone, *Nano Lett.* **2013**, *13*, 3218 – 3224; d) A. M. Katzenmeyer, V. Aksyuk, A. Centrone, *Anal. Chem.* **2013**, *85*, 1972 – 1979; e) J. R. Felts, K. Kjoller, M. Lo, C. B. Prater, W. P. King, *ACS Nano* **2012**, *6*, 8015 – 8021; f) A. Dazzi, F. Glotin, R. Carminati, *J. Appl. Phys.* **2010**, *107*, 124519; g) A. Dazzi, R. Prazeres, F. Glotin, J. M. Ortega, *Infrared Phys. Technol.* **2006**, *49*, 113 – 121.

[14] C. Volkringer, M. Meddouri, T. Loiseau, N. Guillou, J. Marrot, G. Férey, M. Haouas, F. Taulelle, N. Audebrand, M. Latroche, *Inorg. Chem.* **2008**, *47*, 11892 – 11901.

[15] S. Furukawa, K. Hirai, Y. Takashima, K. Nakagawa, M. Kondo, T. Tsuruoka, O. Sakata, S. Kitagawa, *Chem. Commun.* **2009**, 5097 – 5099.

[16] T. Fukushima, S. Horike, H. Kobayashi, M. Tsujimoto, S. Isoda, M. L. Foo, Y. Kubota, M. Takata, S. Kitagawa, *J. Am. Chem. Soc.* **2012**, *134*, 13341 – 13347.

[17] R. J. T. Houk, B. W. Jacobs, F. E. Gabaly, N. N. Chang, A. A. Talin, D. D. Graham, S. D. House, I. M. Robertson, M. D. Allendorf, *Nano Lett.* **2009**, *9*, 3413 – 3418.

[18] X. Kong, H. Deng, F. Yan, J. Kim, J. A. Swisher, B. Smit, O. M. Yaghi, J. A. Reimer, *Science* **2013**, *341*, 882 – 885.

[19] C. Marcott, M. Lo, K. Kjoller, C. Prater, I. Noda, *Appl. Spectrosc.* **2011**, *65*, 1145 – 1150.

[20] B. Van Eerdenbrugh, M. Lo, K. Kjoller, C. Marcott, L. S. Taylor, *Mol. Pharm.* **2012**, *9*, 1459 – 1469.

[21] C. Policar, J. B. Waern, M.-A. Plamont, S. Clède, C. Mayet, R. Prazeres, J.-M. Ortega, A. Vessières, A. Dazzi, *Angew. Chem.* **2011**, *123*, 890 – 894; *Angew. Chem. Int. Ed.* **2011**, *50*, 860 – 864.

[22] D. Dubbeldam, K. S. Walton, D. E. Ellis, R. Q. Snurr, *Angew. Chem.* **2007**, *119*, 4580 – 4583; *Angew. Chem. Int. Ed.* **2007**, *46*, 4496 – 4499.

[23] a) A. F. Gross, E. Sherman, S. L. Mahoney, J. J. Vajo, *J. Phys. Chem. A* **2013**, *117*, 3771 – 3776; b) M. Kim, J. F. Cahill, H. Fei, K. A. Prather, S. M. Cohen, *J. Am. Chem. Soc.* **2012**, *134*, 18082 – 18088; c) M. Kim, J. F. Cahill, Y. Su, K. A. Prather, S. M. Cohen, *Chem. Sci.* **2012**, *3*, 126 – 130; d) T. Li, M. T. Kozlowski, E. A. Doud, M. N. Blakely, N. L. Rosi, *J. Am. Chem. Soc.* **2013**, *135*, 11688 – 11691.

[24] a) L. Wu, M. Xue, S.-L. Qiu, G. Chaplais, A. Simon-Masseron, J. Patarin, *Microporous Mesoporous Mater.* **2012**, *157*, 75 – 81; b) M. Savonnet, D. Bazer-Bachi, N. Bats, J. Perez-Pellitero, E. Jeanneau, V. Lecocq, C. Pinel, D. Farrusseng, *J. Am. Chem. Soc.* **2010**, *132*, 4518 – 4519.

[25] R. N. Jones, C. Sandorfy in *Technique of Organic Chemistry*, *Vol. IX* (Ed.: A. Weissberger), Interscience, New York, **1956**.

